Electronic Supplementary Information (ESI) for

High-spin versus spin-crossover versus low-spin: geometry intervention in cooperativity in a 3D polymorphic iron(II)-tetrazole MOFs system

Zheng Yan,‡ Mian Li,‡ Hui-Ling Gao, Xiao-Chun Huang* and Dan Li*

Department of Chemistry, Shantou University, Guangdong 515063, P. R. China.

E-mail: xchuang@stu.edu.cn, dli@stu.edu.cn

‡ These authors contributed equally to this work.

Contents

Experimental Section

General: Reagents and solvents employed were commercially available and used as received. The ligand 5,5'-(1,4-phenylene)bis(1*H*-tetrazole) (H_2bpt) was prepared by the method reported in previous work.[1] Infrared spectra were obtained in KBr disks on a Nicolet Avatar 360 FTIR spectrometer in the range of 4000-400 cm^{-1}; abbreviations used for the IR bands are w = weak, m = medium, b = broad, vs = very strong. Thermogravimetric measurements were performed on a TA Instruments Q50 Thermogravimetric Analyzer under nitrogen flow of (40 $mL\cdot min^{-1}$) at a typical heating rate of 10 $°C\cdot min^{-1}$. X-ray powder diffraction (XRPD) experiments were performed on a D8 Advance X-ray diffractometer. Magnetization measurements were performed on phase-pure samples from crushed single crystals using a Quantum Design MPMS-XL7 SQUID.

Synthesis of 1: A solution of $FeSO_4\cdot 7H_2O$ (0.056 g, 0.2 mmol), H_2bpt (0.084 g, 0.3 mmol), NaSCN (0.032 g, 0.4 mmol) in <u>isopropanol (6 mL) and cyclohexane (2 mL)</u> was sealed in a 15 mL Teflon-lined reactor and heated at 160 ºC for 3 days and then cooled to room temperature at a rate of 5 ºC/h. Subsequently, prismatic pale colourless crystals were obtained in 78 % yield based on Fe. IR (KBr pellet, cm^{-1}): 3491 (m), 1605 (w), 1495 (s), 1438 (w), 1387 (m), 1274 (w), 1235 (s), 1145(w), 1068 (w), 1016 (w), 972 (w), 849 (w), 808 (w), 751 (m), 554 (m), 492 (s). Elemental analysis calcd (%) $C_{24}H_{22}O_4N_{24}Fe_2$: C, 35.06; H, 2.70; N, 40.88. found: C, 35.22; H, 2.59; N, 39.83.

Synthesis of 2: A solution of $FeSO_4\cdot 7H_2O$ (0.056 g, 0.2 mmol), H_2bpt (0.084 g, 0.3 mmol), NaSCN (0.032 g, 0.4 mmol) in <u>isopropanol (8 mL) and water (1 mL)</u> was sealed in a 15 mL Teflon-lined reactor and heated at 160 ºC for 3 days and then cooled to room temperature at a rate of 5 ºC/h. Subsequently, plate-like pale red crystals were obtained in 65% yield based on Fe. IR (KBr pellet, cm^{-1}): 3407 (m), 1635 (w), 1438 (s), 1386 (w), 1351 (m), 1273 (w), 1198 (s), 1156(w), 1107 (w), 1064 (w), 1011 (w), 856 (w), 755 (w), 549 (m), 500 (m). Elemental analysis calcd (%) $C_{24}H_{40}O_{13}N_{24}Fe_2$: C, 29.28; H, 4.10; N, 34.15. found: C, 30.22; H, 3.97; N, 34.62.

Synthesis of 3: A solution of $FeSO_4\cdot 7H_2O$ (0.056 g, 0.2 mmol), H_2bpt (0.084 g, 0.3 mmol), NaSCN (0.032 g, 0.4 mmol) in <u>isopropanol (5 mL) and water (3 mL)</u> was sealed in a 15 mL Teflon-lined reactor and heated at 160 ºC for 3 days and then cooled to room temperature at 5 ºC/h. Subsequently, prismatic dark crystals were obtained in 35% yield based on Fe. IR (KBr pellet, cm^{-1}): 3355 (m), 1629 (w), 1441 (s), 1384 (w), 1271 (m), 1228 (w), 1114 (s), 1067(w), 1033 (w), 1010 (w), 856 (w), 771 (w), 755 (w), 560 (m), 477 (m). Elemental analysis calcd (%) $C_{24}H_{44}O_{15}N_{24}Fe_2$: C, 28.25; H, 4.35; N, 32.94. found: C, 28.01; H, 4.18; N, 32.14.

Note: Sometimes concomitant polymorphism occurred in the above given conditions, which were optimized to ensure the relatively higher yield for each compound.

---

[1] J. Tao, Z.-J. Ma, R.-B. Huang, L.-S Zheng, *Inorg. Chem.*, 2004, **43**, 6133-6135.

Crystal Data Section

Crystallography: Both room-temperature (**1**, **2** and **3**) and cryogenic (**1'**, **2'** and **3'**) structures were measured. Suitable crystals of **1**, **1'**, **2**, **2'**, **3** and **3'** were mounted with glue at the end of a glass fiber, respectively. Data collection was performed on a Bruker Smart Apex CCD diffractometer (Mo Kα, λ = 0.71073 Å) using SMART [Bruker AXS, Madison, WI, USA, **1997**]. Reflection intensities were integrated using SAINT software and absorption correction was applied semi-empirically [Bruker AXS, Madison, WI, USA, **1997**]. The structures were solved by direct methods and refined by full-matrix least-squares refinements based on F^2. Anisotropic thermal parameters were applied to all non-hydrogen atoms. The hydrogen atoms were generated geometrically (C-H = 0.960 Å). The crystallographic calculations were conducted using the SHELXL-97 programs.[2] The benzene ring group in **1**, **1'**, **2**, **2'**, **3** and **3'** was found to be disordered. The treatment for the guest molecules in **1-3** involved the use of the SQUEEZE program of PLATON.[3] Parameters for data collection and refinement of complexes **1**, **1'**, **2**, **2'**, **3** and **3'** are summarized in Table S1. Selected bond lengths and angles for complexes **1**, **1'**, **2**, **2'**, **3** and **3'** are given in Table S2. Table S3 provides a comparison of the key structural parameters (Fe–N bond lengths and distortion indices) of room-temperature and cryogenic structures.

Note: The charge balance of all three complexes requires that 2/3 of the ligands remain singly protonated in the form of Hbdt at the N2 or N4 site, as previously described in an analogous complex, namely $[Co_2(H_{0.67}bdt)_3]\cdot 20H_2O$.[4] Although the crystallography did not reveal the protonation sites owing to symmetry and occupational considerations, the final electron density maps, as well as IR spectroscopy, confirmed the absence of other potential charge compensating groups.

Topological Analysis: The point symbols[5] and vertex symbols[5] are computed using *OLEX*[6] and *TOPOS*.[7] Comprehensive topological network analyses are performed using Systre.[8] The three-letter symbols for nets are based on the recommendation of *RCSR*.[9]

---

[2] G. M. Sheldrick, *Acta Crystallogr.*, 2008, **A64**, 112-122.
[3] A. Spek, *J. Appl. Crystallogr.*, 2003, **36**, 7-13.
[4] W. Ouellette, A. V. Prosvirin, K. Whitenack, K. R. Dunbar, J. Zubieta, *Angew. Chem., Int. Ed.*, 2009, **48**, 2140-2143.
[5] V. A. Blatov, M. O'Keeffe, D. M. Proserpio, *CrystEngComm*, 2010, **12**, 44-48.
[6] O. V. Dolomanov, A. J. Blake, N. R. Champness, M. J. Schröder, *Appl. Crystallogr.*, 2003, **36**, 1283. The program packages are available at: http://www.ccp14.ac.uk/ccp/web-mirrors/lcells/olex_index.htm.
[7] V. A. Blatov, *Multipurpose crystallochemical analysis with the program package TOPOS. IUCr CompComm Newsletter* **2006**, *7*, 4-38. *TOPOS* is available at http://www.topos.ssu.samara.ru.
[8] O. Delgado-Friedrichs, M. O'Keeffe, *Acta Crystallogr.*, 2003, **A59**, 351-360. Website: http://www.gavrog.org/.
[9] M. O'Keeffe, M. A. Peskov, S. J. Ramsden, O. M. Yaghi, *Acc. Chem. Res.*, 2008, **41**, 1782-1789. Website: http://rcsr.anu.edu.au/.

Table S1. Summary of the Crystal Data and Structure Refinement Parameters for **1**, **1'**, **2**, **2'**, **3** and **3'**.

Parameter	**1**	**1'**	**2**	**2'**	**3**	**3'**
Formula	$C_{12}H_7FeN_{12}$	$C_{12}H_7FeN_{12}$	$C_{12}H_7FeN_{12}$	$C_{12}H_7FeN_{12}$	$C_{12}H_7FeN_{12}$	$C_{12}H_7FeN_{12}$
Fw.	375.15	375.15	375.15	375.15	375.15	375.15
Space group	*Fddd*	*Fddd*	*R*-3*m*	*R*-3	*Cmmm*	*Cmmm*
a (Å)	7.8304(2)	7.7980(3)	22.604(4)	22.4652(8)	7.2772(7)	7.2589(5)
b (Å)	26.310(5)	26.306(1)	22.604(4)	22.4652(8)	25.796(3)	25.762(2)
c (Å)	30.543(6)	30.399(1)	7.454(3)	7.3495(3)	12.246(1)	12.2049(9)
V ($Å^3$)	6292(2)	6235.9(5)	3298(2)	3212.3(3)	2298.9(4)	2282.4(3)
Z	16	16	6	6	4	4
T(K)	293(2)	100(2)	293(2)	100(2)	293(2)	100(2)
D_{calcd} ($g{\cdot}cm^{-3}$)	1.584	1. 598	1.133	1.164	1.084	1.092
Ref. collected	8307	4775	4664	2974	5388	4080
Ref. unique	1401	1384	709	1561	1164	1445
R_{int}	0.0339	0.0390	0.0412	0.0248	0.0372	0.0658
GOF	1.092	1.053	1.042	1.110	1.163	1.007
$R_1{}^a$ $[I > 2\sigma(I)]$	0.0336	0.0315	0.0399	0.0435	0.0580	0.0535
$wR_2{}^b$ [all data]	0.0940	0.0756	0.1165	0.1157	0.1499	0.1413
max,min peaks ($eÅ^{-3}$)	0.464, -0.272	0.434, -0.291	0.466, -0.330	0.418,-0.539	0.868,-0.585	0.654, -0.406

[a] $R_1 = \sum|F_o| - |F_c||/\sum|F_o|$. [b] $wR_2 = \{[\sum w(F_o^2-F_c^2)^2]/\sum[w(F_o^2)^2]\}^{1/2}$; $w = 1/[\sigma^2(F_o^2) + (aP)^2 + bP]$, where $P = [\max(F_o^2,0) + 2F_c^2]/3$ for all data.

Table S2. Selected Bond Lengths (Å) and Bond Angles (°) for **1**, **1'**, **2**, **2'**, **3** and **3'**.[a]

Complex **1**			
Fe(1)-N(1)	2.156(2)	Fe(1)-N(3)	2.234(2)
Fe(1)-N(4)#1	2.248(2)	N(1)-Fe(1)-N(1)#2	174.5(1)
N(1)-Fe(1)-N(3)#2	90.24(7)	N(1)#2-Fe(1)-N(3)#2	93.27(7)
N(3)#2-Fe(1)-N(3)	101.2(1)	N(3)-Fe(1)-N(4)#1	172.12(7)
N(1)-Fe(1)-N(4) #1	88.87(7)	N(1)#2-Fe(1)-N(4) #1	87.10(7)
N(3)#2-Fe(1)-N(4) #1	86.33(7)	N(4)#1-Fe(1)-N(4)#3	86.2(1)
Complex **1'**			
Fe(1)-N(1)	2.145(2)	Fe(1)-N(6)#2	2.219(2)
Fe(1)-N(3)	2.231(2)	N(1)-Fe(1)-N(1)#1	174.0(1)
N(1)-Fe(1)-N(6)#2	90.27(7)	N(1)#1-Fe(1)-N(6)#2	93.50(7)
N(6)#2-Fe(1)-N(6)#3	102.1(1)	N(1)-Fe(1)-N(3)	87.28(7)
N(1)#1-Fe(1)-N(3)	88.32(7)	N(6)#2-Fe(1)-N(3)	171.46(8)
N(6)#3-Fe(1)-N(3)	86.20(7)	N(3)-Fe(1)-N(3)#1	85.6(1)
Complex **2**			
Fe(1)-N(3)	1.963(3)	Fe(2)-N(2)	2.170(3)
N(3)#1-Fe(1)-N(3)	87.9(1)	N(2)#2-Fe(2)-N(2)	93.1(1)
Complex **2'**			
Fe(1)-N(3)	1.950(2)	Fe(2)-N(2)	2.099(2)
N(3)#2-Fe(1)-N(3)	91.03(8)	N(2)-Fe(2)-N(2)#1	92.00(8)
Complex **3**			
Fe(1)-N(2)	1.953(4)	Fe(1)-N(4)	1.968(3)
N(2)-Fe(1)-N(4)#1	90.9(1)	N(4)-Fe(1)-N(4)#2	90.7(2)
Complex **3'**			
Fe(1)-N(2)	1.948(3)	Fe(1)-N(4)	1.961(2)
N(2)-Fe(1)-N(4)#2	89.18(9)	N(4)#2-Fe(1)-N(4)#1	91.0(1)

[a] Symmetry codes for **1**: #1 x-1/2,-y+3/4,-z+1/4; #2 -x+3/4,-y+3/4,z; #3 -x+5/4,y,-z+1/4; for **1'**: #1 -x+3/4,-y+3/4,z; #2 x-1/2,-y+3/4,-z+1/4; #3 -x+5/4,y,-z+1/4; for **2**: #1 x-y+2/3,x+1/3,-z+1/3; #2 x-y+2/3,x+1/3,-z+4/3; for **2'**: #1 x-y,x,-z; #2 -y,x-y,z; for **3**: #1 -x+1/2,-y+1/2,-z+1; #2 -x+1/2,-y+1/2,z; for **3'**: #1 -x+1/2,-y+1/2,-z; #2 x,y,-z.

Table S3. Comparison of Key Structural Parameters of Room-Temperature and Cryogenic Structures.

Complex	Colour	Space Group	<Fe–N> (Å) [a]	Σ (°) [b]
1 (293 K)	colourless	*Fddd*	2.213(2)	37.5
1' (100 K)	colourless	*Fddd*	2.198(2)	40.5
2 (293 K)	red	*R-3m*	**2.170(3)** 1.963(3)	**37.2** **25.2**
2' (100 K)	black	*R-3*	**2.099(2)** 1.950(2)	**24.0** **12.4**
3 (293 K)	black	*Cmmm*	1.961(4)	10.0
3' (100 K)	black	*Cmmm*	1.955(3)	10.7

[a] <Fe–N>: average of the six Fe–N bond lengths around each octahedral Fe center. [b] Σ is the sum of the deviation from 90 ° of the twelve *cis*-N–Fe–N angles about the Fe center; it is a general measure of the deviation of a metal ion from an ideal octahedral geometry.[10]

The above comparison gives some useful information as below:

1) HS bond lengths are significantly longer (normally *ca.* 0.2 Å) than LS bong lengths, and the LS octahedral configuration is more regular than that of HS, which is consistent with the theoretical aspect that the lower number of antibonding e_g* electrons in LS state results in stronger metal-ligand bonding, and thus a less deformable coordination sphere.

2) Only the Fe–N bond lengths of the HS site in **2** are significantly shorten upon cooling, suggesting SCO may occur in this site.

3) The supposedly LS site in **2**, though with no obvious bond contraction, exhibits more regular coordination geometry at low temperature, suggesting it may be partially HS and contribute to the magnetic moments, and thus undergoes partial SCO.

Further explanation for the magnetic data of **2**:

Our first clue to the interpretation that a small proportion of the green site also contributes is the magnetic data of **3** (it contributes to the magnetic moment), and a very similar local Fe^{II} geometry between **3** (1.961(4) Å at RT, 1.955(3) Å at 100 K) and the green site of **2** (1.963(3) Å at RT, 1.950(2) Å at 100 K). The distortion at 100 K is also approached (*ca*. 12.4 for **2**, 10.7 for **3**). We speculate the dramatic change of the distortion parameters for the green site in **2** is due to the structural correlation of the green site and the red site. Very interestingly, at RT the distortion of the red site (*ca*. 37.2) is close to that of **1** (*ca*. 37.5), but at 100 K the distortion of the red site (*ca*. 24.0) is obviously larger for low spin, approaching that of the green site at RT (*ca*. 25.2). This is another structural proof for the correlation of the green and red sites, thus influencing the overall spin state behavior of **2**. In the

[10] M. A. Halcrow, *Chem. Soc. Rev.*, 2011, **40**, 4119-4142.

future, some key points, being the structure information of the intermediate state, should be added for further discussion.

Structural Description Section

Principle of topological analysis (rod SBU approach):

There is no generally agreed way of analyzing the topology of materials such as MOFs. Here we adopt the procedure preferred by O'Keeffe and Yaghi[11] of first identifying the *points of extension* of the links to cations. In the present work in each structure tetrazole rings are linked to two metal atoms and the carbon of the tetrazole ring is the point of extension. O'Keeffe and Yaghi next identify the metal-containing secondary building unit (SBU) as defined by metal atoms that have at least one point of extension in common. The SBU is the shape (in mathematical terms, the *convex* hull) defined by the ensemble of these points. From this point of view the SBU consists of infinite rods of Fe atoms, and the points of extension are the vertices of a column of octahedral sharing opposite faces as shown in Fig. S2e. O'Keeffe and Yaghi in fact identified exactly this SBU in a copper triazolate/tetrazolate MOF reported by Bondar *et al.*.[12]

The three structures studied here all have the same SBU and their nets represent different ways of linking columns of octahedra to form 7-coordinated nets. In **1** a new binodal net with symmetry *Fddd* is formed and to which the *RCSR* symbol[9] of **yzh** has been assigned. As far as we know this topology has not been reported before for a crystalline material. In **2** the net is uninodal, with symmetry $R\bar{3}m$. This net, with RCSR symbol **wnf** is illustrated by O'Keeffe and Yaghi,[11] but again as far as we know, has not before been described as the topology of a real material. In **3** the topology is that of the binodal net with *RCSR* symbol **oab**, which O'Keeffe and Yaghi[11] identified as the underlying net of structure **8** of Bondar *et al.*.[12]

Prior to the work of O'Keeffe and Yaghi the rod SBU identified here appears not to be recognized before although those authors point out that it also occurs in scandium terephthalate[13] with yet another binodal net with *RCSR* **sct**[11] and again with symmetry *Fddd*. However the authors of that work placed the nodes of the underlying net in the centers of the shared faces of the octahedral to produce a 5-coordinated net which they used to describe the topology.

Yet another approach to finding the underlying topology is that espoused by Alexandrov *et al.*[14] using the program *TOPOS*. In what they call the "standard representation" they consider the metal atoms as 6-coordinated vertices and the linker (which is connected to four metal atoms) as a 4-coordinated vertex to obtain a (4,6)-coordinated net. O'Keeffe and Yaghi[11] pointed out that in this approach the linker should be considered as two 3-coordinated nodes and the net should be (3,6)-coordinated and the net **tsy** in *RCSR*.

---

[11] M. O'Keeffe, O. M. Yaghi, *Chem. Rev.*, 2012, **112**, DOI: 10.1021/cr200205j.
[12] O. A. Bondar, L. V. Lukashuk, A. B. Lysenko, H. Krautscheid, E. B. Rusanov, A. N. Chernega, K. V. Domasevitch, *CrystEngComm*, 2008, **10**, 1216-1226.
[13] (a) J. Perles, M. Iglesias, M.-Á. Martin-Liengo, M. Á. Monge, C. R. Valero, N. Snejko, *Chem. Mater.*, 2005, **17**, 5837-5842; (b) S. R. Miller, P. A. Wright, C. Serre, T. Loiseau, J. Marrot, G. Férey, *Chem. Commun.*, 2005, 3850-3852.
[14] E. V. Alexandrov, V. A. Blatov, A. V. Kochetkov, D. M. Proserpio, *CrystEngComm*, 2011, **13**, 3947-3958.

Description of structure 1:

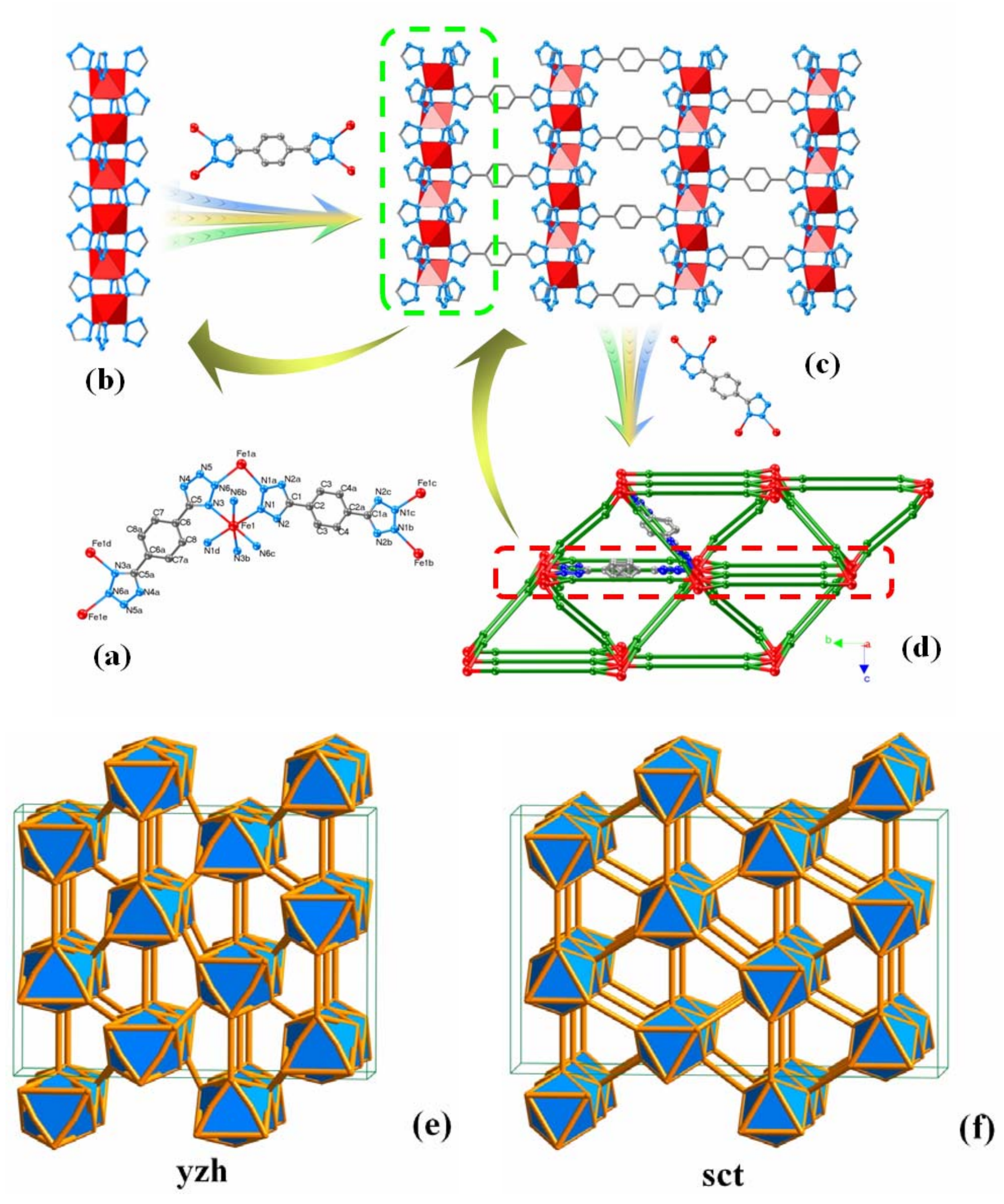

Fig. S1. Representations of the structure of **1**. (a) Coordination environment of the Fe^{II} ion. (b) Polyhedron-and-stick representation of the 1D Fe^{II}-tetrazole building block; note there are both 2,3- and 1,2-bridging sites. (c) View of the 2D layer formed from the 1D Fe^{II}-tetrazole chains linked via the 2,3-bridging ligands. (d) Topological representation of the 3D (3,6)-connected net. One 2,3-bridging ligand and one 1,2-bridging ligand are shown in the network. (e) Topological representation of the binodal 7-connected **yzh** net. (f) Topological representation of a closely-related net **sct** which has the same symmetry (*Fddd*).

Isomer **1** crystallizes in the orthorhombic space group of *Fddd*, and contains one independent Fe^{II} ion, as well as one and a half ligand H_2bpt in the asymmetric unit (Fig. S1a). The Fe1 atom is in a distorted octahedral arrangement comprised of two terminus nitrogen donors (N1 and N1a), two terminus (N3 and N3a), and two edge nitrogen donors (N6 and N6a), with the angles varying from 86.2(1) to 101.2(1)°. The Fe–N bond lengths are in the range of 2.156(2)–2.248(2) Å. The ligand can be considered as a tetradentate linker through four terminal N showing both 2,3- and 1,2-edge-bridging modes. The triply-bridged Fe^{II}-tetrazole 1D building blocks (Fig. S1b) (with a Fe···Fe separation of *ca.* 3.94 Å) running along the *a* axis are linked via the 2,3-bridging ligands to form a 2D layer (Fig. S1c) parallel to the *ab* plane. These 2D layers are further connected by two sets of 1,2-bridging ligands (with the inclined mode) to generate a 3D framework. By viewing each bistetrazolate ligand as two linked 3-connected nodes, and each Fe ion as a 6-connected node, a 3D (3,6)-connected net (Fig. S1d) can be generated. The Point Symbol is $(4.8.9)_3(4.9.10)_3(4^6.8^3.9.10^5)_2$, and the Vertex Symbol is $(4_2.8.9)_3(4_2.9_2.10_9)_3(4.4.4.4.4.4.8.8.8.9.10_6.10_6.10_6.10_3.10_6)_2$. As pointed out in the above topological analysis principle, a more visually and practically reasonable procedure by identifying the rod SBU of linked octahedra would give a new binodal 7-connected net **yzh** (Fig. S1e), which is closely related to the **sct** net (Fig. S1f) with the same symmetry. The **yzh** net is a squashed version of the **sct** net, and the inclined mode (through the 1,2-bridging sites) of the bistetrazole ligand links two slipped octahedra in the neighboring chain-like building blocks and thus makes a difference in topology.

Description of structure 2:

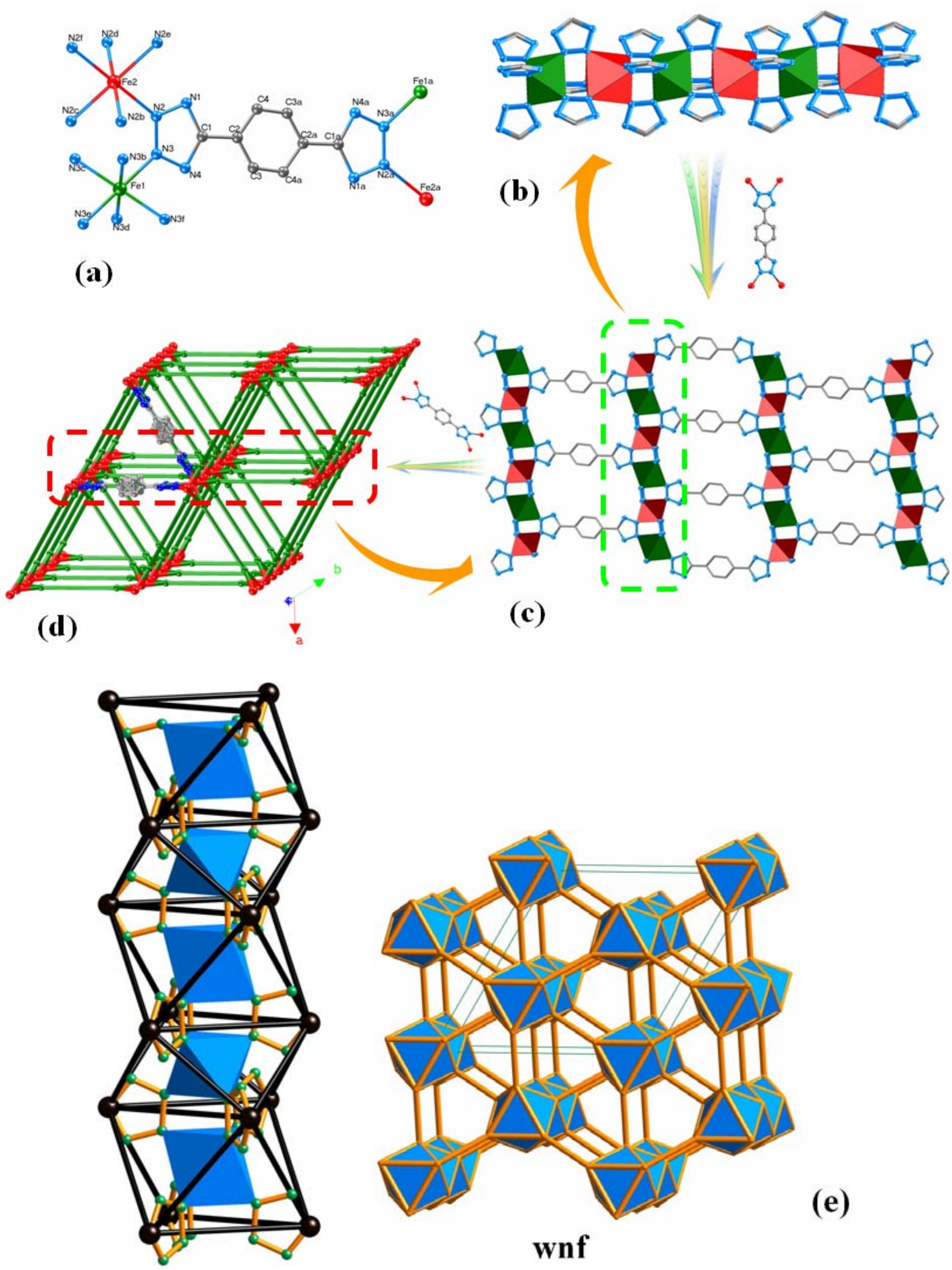

Fig. S2. Representations of the structure of **2**. (a) Coordination environment of the two distinct Fe^{II} ions. (b) Polyhedron-and-stick representation of the 1D Fe^{II}-tetrazole building block; note the two distinct Fe^{II} sites are shown in red and green polyhedral, respectively. (c) View of the 2D layer formed from the 1D Fe^{II}-tetrazole chains linked via the 2,3-bridging ligands. (d) Topological representation of the 3D (3,6)-connected net. Two 2,3-bridging ligands are shown in the network. (e) The rod SBU of linked octahedra (left) and topological representation of the uninodal 7-connected **wnf** net (right).

Isomer **2** crystallizes in the hexagonal space group of *R*-3*m*, and, unlike in **1** and **3**, contains two distinct Fe^{II} ions, as well as one and a half ligand H_2bpt in the asymmetric unit (Fig. S2a). For Fe1, the Fe–N bond length is shorter (Fe1–N = 1.963(3) Å), with the angles 87.9(1) °; for Fe2, the Fe–N bond length is longer (Fe2–N = 2.170(3) Å), with the angles 93.1(1) °. The ligand in **2** only displays 2,3-edge-bridging mode. The triply-bridged Fe^{II}-tetrazole 1D building blocks (Fig. S2b) (with a Fe···Fe separation of *ca.* 3.73 Å) running along the *c* axis are linked via three sets of 2,3-bridging ligands to form a 3D hexagonal framework which contains 2D layers (Fig. S2c) parallel to the three crystal axes. By viewing each bistetrazolate ligand as two linked 3-connected nodes, and each Fe ion as a 6-connected node, a 3D (3,6)-connected net (Fig. S2d) can be generated. The Point Symbol is $(4.9^2)_6(4^6.9^6.10^3)_2$, and the Vertex Symbol is $(4_2.9_2.9_4)_6(4.4.4.4.4.4.9.9.9.9.9.9.10_6.10_6.10_6)(4.4.4.4.4.4.9_2.9_2.9_2.9_2.9_2.9_2.10_6.10_6.10_6)$. According to the rod SBU approach, the framework of **2** can be deconstructed into its underlying net of uninodal 7-connected **wnf** (Fig. S2e).

Description of structure 3:

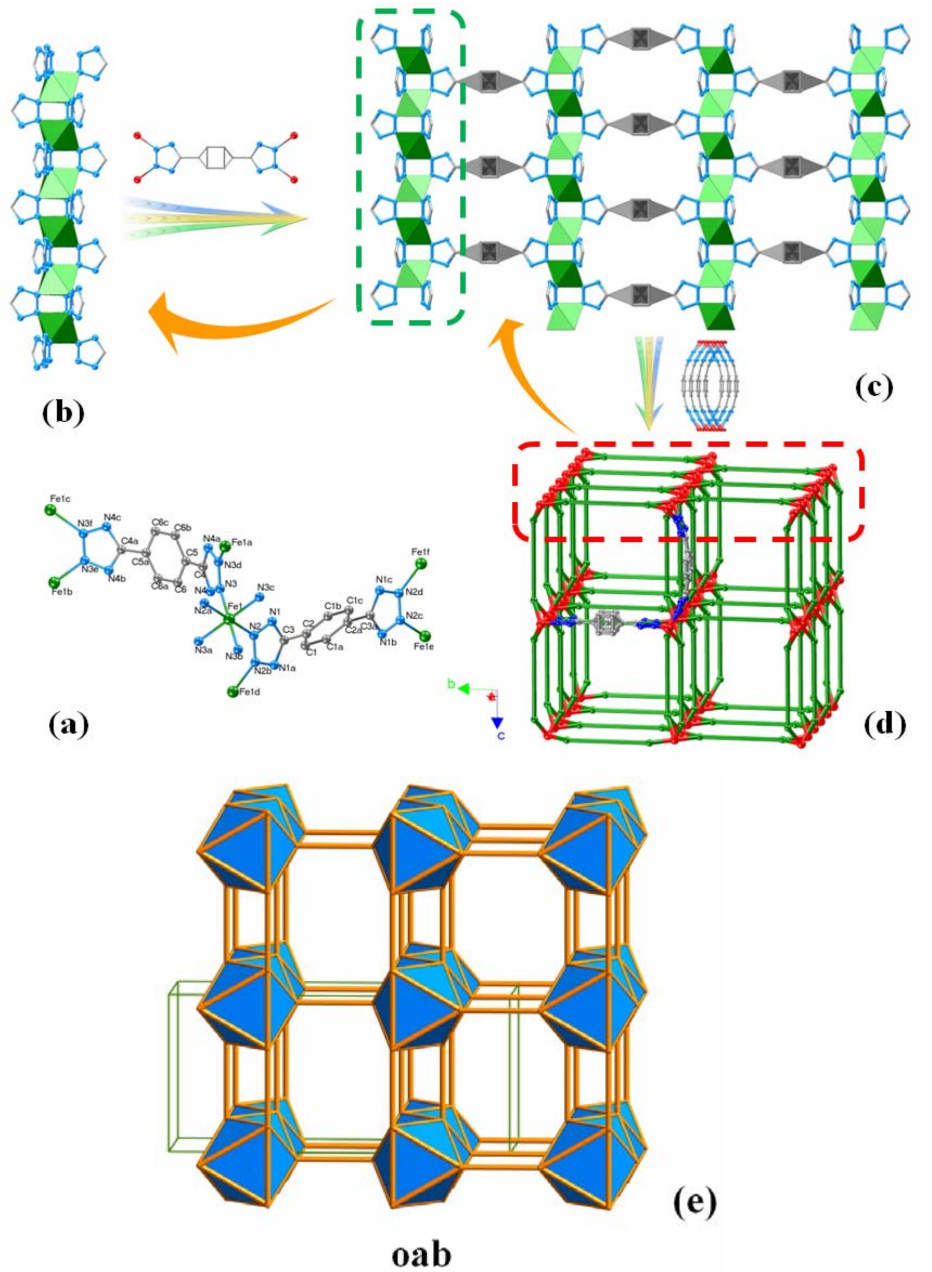

Fig. S3. Representations of the structure of **3**. (a) Coordination environment of the Fe^{II} ion. (b) Polyhedron-and-stick representation of the 1D Fe^{II}-tetrazole building block. (c) View of the 2D layer formed from the 1D Fe^{II}-tetrazole chains linked via the 2,3-bridging ligands. (d) Topological representation of the 3D (3,6)-connected net. Two 2,3-bridging ligands, including a straight one and a bent one, are shown in the network. (e) Topological representation of the binodal 7-connected **oab** net.

Isomer **3** crystallizes in the orthorhombic space group of *Cmmm*, and only contains one independent Fe^{II} ion, as well as one and a half ligand H_2bpt in the asymmetric unit (Figure S3a). The Fe1 atom is in a slightly distorted octahedral arrangement with the Fe−N bond lengths 1.953(4) and 1.968(3) Å and angles varying from 90.9(1) and 90.7(2) °. The ligand in **3** also only displays 2,3-edge-bridging mode. The triply-bridged Fe^{II}-tetrazole 1D building blocks (Fig. S3b) (with a Fe···Fe separation of *ca*. 3.73 Å) running along the *a* axis are linked via the straight 2,3-bridging ligands to form a 2D layer (Fig. S3c) parallel to the *ab* plane. These 2D layers are further connected by two sets of bent 2,3-bridging ligands to generate a 3D framework. By viewing each bistetrazolate ligand as two linked 3-connected nodes, and each Fe ion as a 6-connected node, a 3D (3,6)-connected net (Fig. S3d) can be generated. The Point Symbol is $(4.6^2)_3(4.10^2)_3(4^6.6^2.8^6.10)_2$, and the Vertex Symbol is $(4_2.6.6)_3(4_2.10_9.10_9)_3(4.4.4.4.4.4.6.6.10_3.10_6.10_3.10_3.10_3)_2$. According to the rod SBU approach, the framework of **3** can be deconstructed into its underlying net of binodal 7-connected **oab** (Fig. S3e).

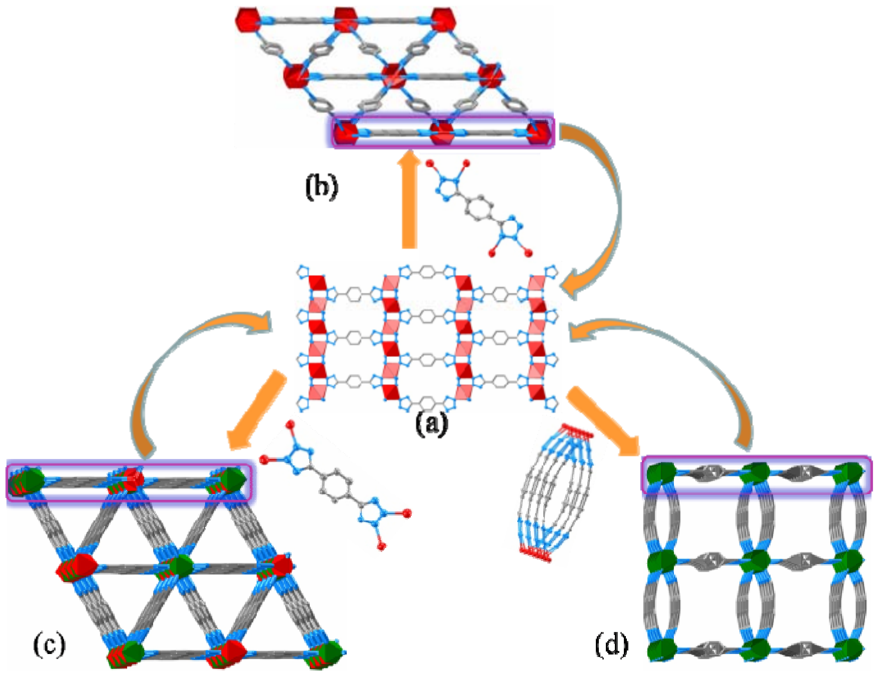

Fig. S4. Representation showing the key linkage difference between the framework of **1** (b), **2** (c) and **3** (d). They are all constructed from 2D layers (a) form by linking the 1D Fe^{II}-tetrazole building block via 2,3-bridging ligands, but are further connected via sets of 1,2-bridging ligands (**1**), straight 2,3-bridging ligands (**2**) and bent 2,3-bridging ligands (**3**), respectively.

Physical Measurement Section

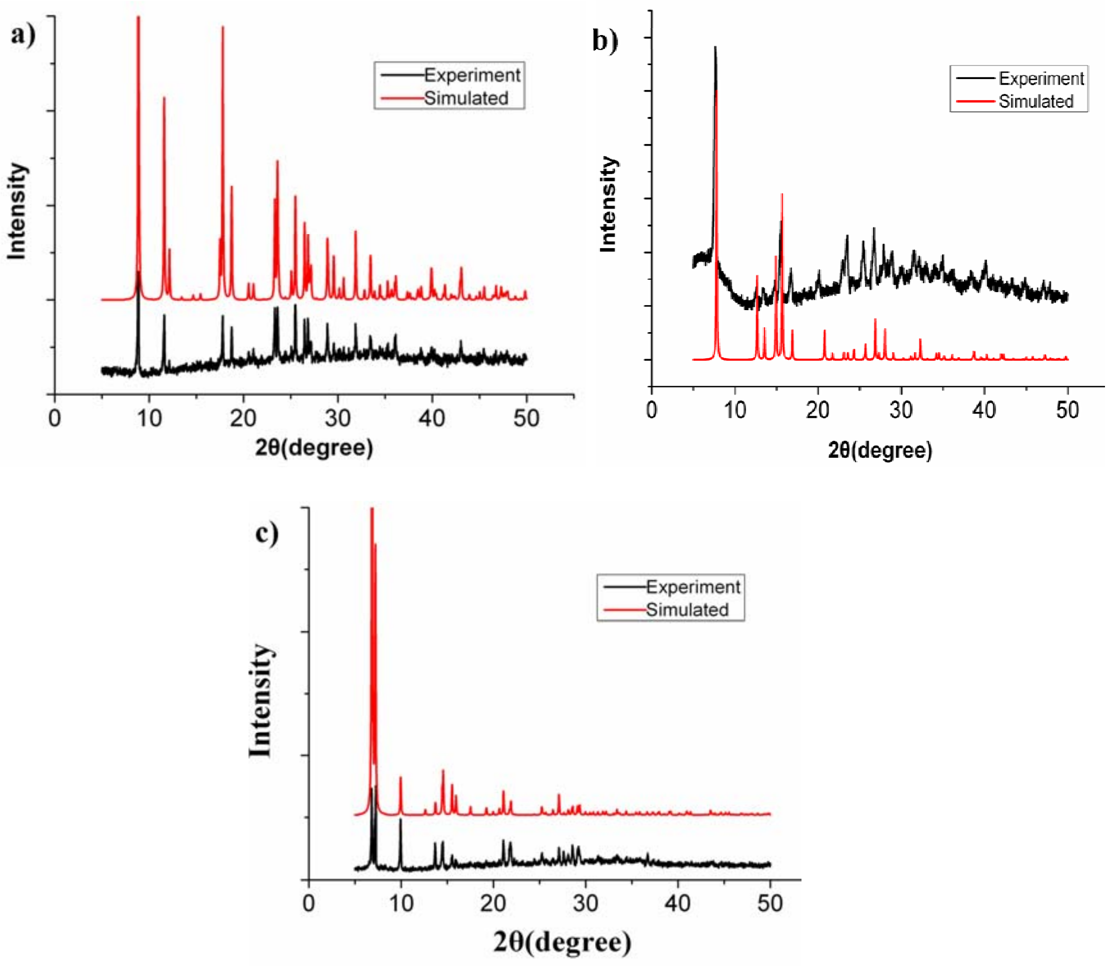

Fig. S5. X-ray powder diffraction patterns: (a)–**1**, (b)–**2**, (c)–**3**. Red: calculated from X-ray single-crystal data; black: as-synthesized data.

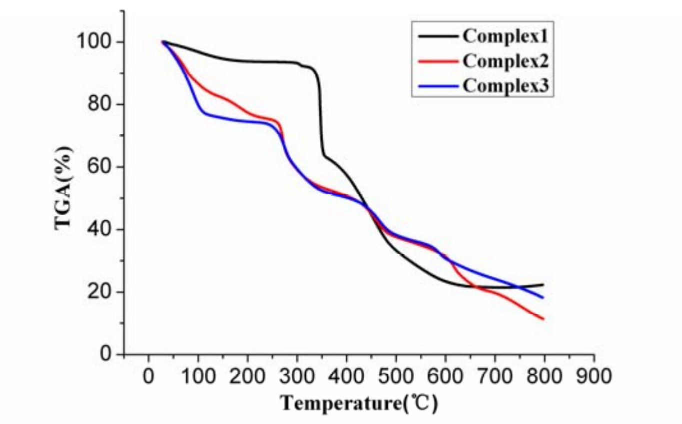

Fig. S6. TGA plots of complexes **1-3** at the temperature range of 30-800 °C [black–**1**, red–**2**, blue–**3**].

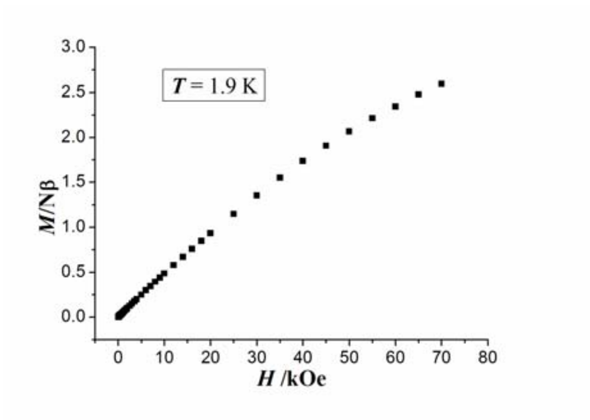

(a)

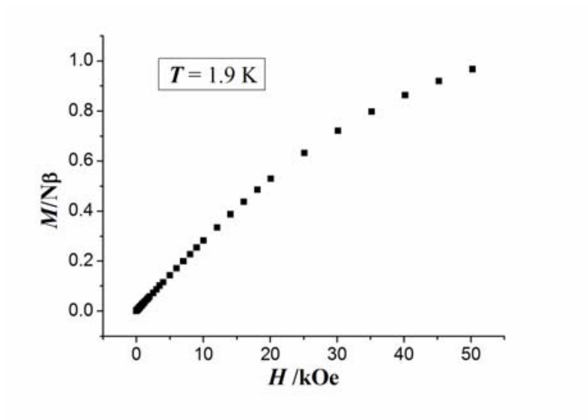

(b)

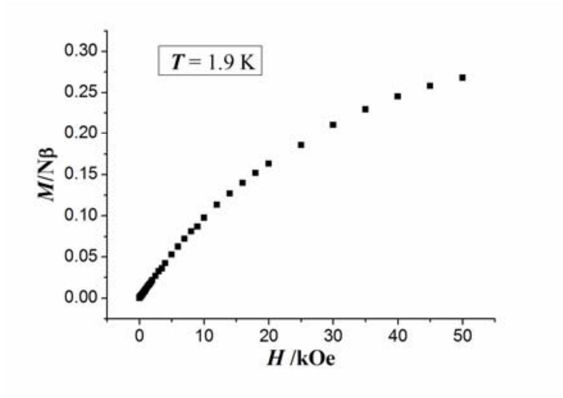

(c)

Fig. S7. M vs H plots of complexes **1** (a), **2** (b) and **3** (c).